A Microfluidic-based Tactile Sensor for Palpating Mice Tumor Tissues

Yichao Yang[1], Garett Johnson[2], Dean Krusienski[2], Siqi Guo[3], Cheng Lin[4] and Zhili Hao[1]
[1]*Department of Mechanical and Aerospace Engineering, Old Dominion University, Norfolk, VA, U.S.A.*
[2]*Department of Electrical and Computer Engineering, Old Dominion University, Norfolk, VA, U.S.A.*
[3]*Center of BioElectrics, Old Dominion University, Norfolk, VA, U.S.A.*
[4]*Department of Engineering Technology, Old Dominion University, Norfolk, VA, U.S.A.*

Keywords: Microfluidics, Tactile Sensor, Transducer Array, Tumor Localization, Minimally Invasive Surgery.

Abstract: In light of the need of tissue palpation for Robotics-assisted Minimally Invasive Surgery (RMIS), this paper presents a microfluidic-based tactile sensor for palpating mice tissues for tumor localization. The core of the sensor is a 3×3 sensing-plate/transducer array built into a single polydimethylsiloxane (PDMS) microstructure, with a transducer spacing of 3.75mm×1.5mm. Mounted on a robot, the sensor is pressed against a tissue region with a pre-defined indentation depth pattern, and consequently the stiffness distribution across the tissue region translates to the deflection distribution of the sensing-plate array and is captured by the transducer array underneath as resistance changes. Thus, the recorded data on a tissue region is the sensor deflection as a function of the indentation depth. While the continuous manner of the sensor interacting with a tissue region alleviates the error resulting from non-ideal normal contact between the sensor and the tissue region, the error related to uncertainty in contact point is removed by interpreting the palpation results in terms of the slope of the sensor deflection versus the indentation depth. Two mice tumor tissues are palpated using the sensor. After their noise being removed, the raw data on the two tissues are processed to obtain their slope distribution, the slope error and the percentage error in the slope. The slope distribution of each tissue clearly illustrates the location of a tumor. The palpation results also indicate that this sensor can be integrated into a robotic-assisted system for tumor localization.

1 INTRODUCTION

Offering many advantages over open surgeries, Robotic-assisted Minimally Invasive Surgery (RMIS) has gained great popularity over recent years (Girão et al., 2013; Konstantinova et al., 2014; Schostek et al., 2009; Tiwana et al., 2012). With a RMIS system such as the da Vinci™ Surgical System, (Guthart et al., 2000) and the ZEUS™ Surgical System (Uranues et al., 2002), a surgeon gets access to an operation site and performs an operation via robotic-assisted laparoscopic tools through a small incision. Thus, direct manual palpation to a tissue region is lost in RMIS. The lack of tissue palpation not only increases the chance of tissue trauma/damage, but also limits the application of RMIS in many complex procedures (Beccani et al., 2015; Puangmali et al., 2008). Thus, tactile sensors are resorted to for adding tissue palpation to RMIS (Puangmali et al., 2008; Trejos et al. 2009).

Up to date, various tactile sensors have been developed for tissue palpation (Anastassopoulos et al., 2001; Beccani et al., 2015; Panteliou et al., 2000). Since a tumor exhibits a much higher stiffness than its surrounding healthy tissue (Krouskop et al., 1998), tissue palpation via tactile sensors translates to acquiring the stiffness distribution of a tissue region. A tactile sensor is typically comprised of a mechanical structure to convert a force to a deflection and a transducer to register the deflection as an electrical/optical signal. A tissue region is often considered to have the same thickness across it and is much larger than the mechanical structure of a tactile sensor. Thus, the measured stiffness distribution of a tissue region is representative of its elasticity distribution (Anastassopoulos et al., 2001; Konstantinova et al., 2014). Acquiring the stiffness distribution of a tissue region can be achieved either by sliding a tactile sensor over the region or employing a sensor array

Yang, Y., Johnson, G., Krusienski, D., Guo, S., Lin, C. and Hao, Z.
A Microfluidic-based Tactile Sensor for Palpating Mice Tumor Tissues.
DOI: 10.5220/0005705600830092
In *Proceedings of the 9th International Joint Conference on Biomedical Engineering Systems and Technologies (BIOSTEC 2016) - Volume 1: BIODEVICES*, pages 83-92
ISBN: 978-989-758-170-0

to concurrently map out the stiffness distribution of the region (Girão et al., 2013; Konstantinova et al., 2014; Schostek et al., 2009; Tiwana et al., 2012).

In recent years, quite a few MEMS/microfluidic-based tactile sensors and sensor arrays have been incorporated into surgical instruments to enable surgeons to measure mechanical properties (Dargahi and Najarian, 2003; Lanfranco et al., 2004; Ottermo et al., 2006; Su et al., 2012; Talasaz and Patel, 2013;). These studies have greatly advanced the tactile sensing technology and led to a better understanding of its application for tissue palpation. However, two unavoidable misalignment issues (Wanninayake et al., 2013; Zhao et al., 2013) (uncertainty in contact point and non-ideal normal contact) associated with an indiviudal sensor and a sensor array for tissue palpation severely distort the genuine stiffness distribution of a tissue region, yielding false identification of tumors.

To address the misalignment issues, we have developed a two-dimensional (2D) microfluidic-based resistive tactile sensor for tissue palpation (Yang et al., 2015a). The core of the 2D tactile sensor is one whole PDMS microstructure embedded with a 3×3 sensing-plate/transducer array. The distributed deflection acting on the top of the sensing-plate array translates to geometrical changes of the transducer array underneath and further registers as resistance changes. The 2D sensor features ease of fabrication and performance robustness (Yang et al., 2015a). Previously, this sensor has successfully been demonstrated to measure tissue phantoms with embeded dummy tumors. As compared with our previous related work (Yang et al., 2015a), the unique contributions of this paper are 1) the motion of the sensor is controlled by a robot to examine the effect of mounting the sensor on a robot on the palpation results, and 2) two true animal tumor tissues are palpated to examine whether the sensor is suitable for tumor localization of true tumor tissues, instead of well-prepared tumor tissue phantoms.

2 A MICROFLUIDIC-BASED TACTILE SENSOR

2.1 Design and Working Principle

In Figure 1, the configuration of the microfluidic-based tactile sensor is presented. It consists of a PDMS microstructure with a 3×3 circular sensing-plate array at its top and a serpentine-shape electrolyte-filled microchannel at its bottom. A set of electrode pairs are distributed along the microchannel length. The portion of electrolyte underneath a sensing-plate serves as a resistive transducer, whose resistance varies with the bottom deflection of the sensing-plate and is routed out by the electrode pair. Thus, coincident with the sensing-plate array, a 3×3 transducer array is realized by one body of electrolyte in the microchannel and the set of electrode pairs. Distributed deflection acting on top of the microstructure translates to the bottom deflections of the sensing-plates and consequently causes geometrical changes of the transducer array, which register as resistance changes. Two reservoirs at the ends of the microchannel serve as a conduit for electrolyte to flow in/out during the sensor operation. The transducer spacing of the sensing-plate/transducer array is 3.75mm along the x-axis and 1.5mm along the y-axis, respectively. The effective sensing region of the sensor is 7.5 mm×3 mm, defined by the distance between the centers of the sensing-plates at the array sides.

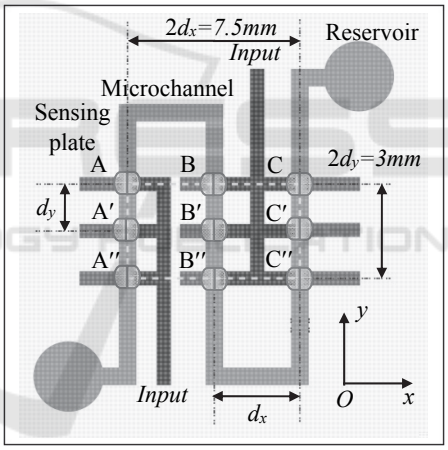

Figure 1: Configuration of a microfluidic-based tactile sensor: a 3×3 sensing-plate/transducer array built into a single PDMS microstructure with transducers being labeled (drawn not to scale for clear illustration).

A standard photolithography fabrication process for PDMS-based microfluidic devices is employed to fabricate the sensor. The microstructure is made of 1:10 PDMS (mixing ratio of cross-linking agent to base of PDMS Sylgard 184 base). Details about the sensor fabrication process can be found in the literature (Gu et al., 2013a). After the sensor is fabricated, electrolyte, 1-ethyl-3-methylimidazolium dicyanamide (EMIDCA), is injected into the microchannel through a hole in the reservoir using a syringe. The holes are then sealed by 1:10 PDMS to prevent leakage of electrolyte for flipping the sensor

over to palpate a tumor tissue. In Figure 2, the fabricated sensor and its sensing-plate/transducer array are shown.

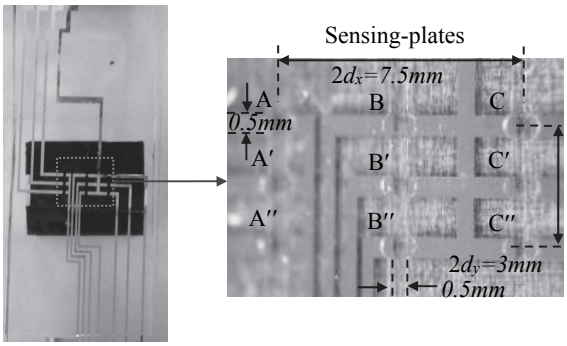

Figure 2: Pictures of (a) the fabricated microfluidic-based sensor (a black paper is put underneath the sensing-plate /transducer array for clear illustration) and (b) close-up view of its sensing-plate/transducer array and electrodes.

2.2 Performance Characterization

The experimental setup (Gu et al., 2013b) used for characterizing the one-dimensional tactile sensor is utilized in this work to characterize the performance of the sensor. The whole experimental setup is implemented on an optical table. The sensor is first mounted on a printed circuit board (PCB) for electrical connections and further fixed on a five-axis manipulator for better position alignment. Mounted on a micropositioner, a cylinder probe of 11mm-in-length and 0.8mm-in-diameter is used to generate distributed deflection on each column of the transducer array, respectively. Note that the applied displacement from the cylinder is the same as the deflection acting on the top of the microstructure, which translates to the bottom deflection of the sensing-plate array and is registered as resistance changes by the transducer array. A six-axis force/torque sensor (NANO 17, ATI Industrial Automation) is incorporated into the experimental setup to monitor the overall force experienced by the tactile sensor, in response to a deflection input.

To monitor the resistance changes of the transducer array, a 100 kHz AC voltage with a peak-to-peak value of 200mv is applied as the common input to all the transducers. The outputs of the transducers are connected to their own electronics with the same design and are converted to DC voltage outputs, which are recorded by a LabVIEW program. The resistance changes can be extracted from the recorded DC voltage outputs (Gu et al., 2013a). Afterward, the resistance changes can be used to find out the bottom deflection of the sensing-plate array (Yang et al., 2015b).

In Figure 3, the average bottom deflection of five measurements of each sensing-plate column as a function of the deflection acting at their tops are presented. A 600μm-indentation depth, z_{in}, exerted on the top of the i^{th} sensing-plate translates to a roughly 12μm-deflection, $z_{s\text{-}i}$, at its bottom (As will be seen in Figure 6). Based on the average slope relation of the top deflection, $z_{top\text{-}i}$, and bottom deflection, $z_{s\text{-}i}$, of the 3×3 sensing-plate array, the deflection at the top of the sensing-plate, $z_{top\text{-}i}$ (equal to z_{in}) is approximately related to its bottom deflection by equation (1).

$$z_{top-i} \cong 58 z_{s-i} \quad (1)$$

The variation in bottom deflection among the sensing-plates is believed to result from in-plane misalignment between the sensor and the cylinder probe, since the fabrication variation in transducer height and the out-of-plane misalignment between the sensor and the probe (the probe being tilt toward one transducer in each column) has been corrected (Yang et al., 2015b). Consequently, the distributed deflections, $z_{top\text{-}i}$, over the contact surface between the sensor and the cylinder probe are captured by the sensor deflection, $z_{s\text{-}i}$. Accompanying the applied distributed deflection, the overall reaction force of the sensor can be obtained from the readout of the six-axis force/torque sensor. The relation ($F\text{-}z_{s\text{-}i}$) between the overall reaction force, F(N), and the sensor deflection, $z_{s\text{-}i}$(μm), is obtained from the slope value of F and $z_{s\text{-}i}$, from a sensing-plate column and is given by equation (2),

$$F \cong 0.116 \cdot z_{s-i} \quad (2)$$

the equation can be used to relate the sensor deflection to the corresponding contact force at a transducer, which is important for avoiding the possible damage to a tumor tissue during palpation.

3 MATERIALS AND METHOD

3.1 Tumor Tissue Preparation

Tumor tissues used in this work were stored at -80°C freezer. The orthotopic mouse breast cancer model was established by injection of 106 4T1-luc cells in 50μL PBS into the left abdominal mammary gland. Tumors were measured every 3 to 4 days by a Caliper and were harvested after one dimension of tumor reached 15 mm diameter then kept at -80°C

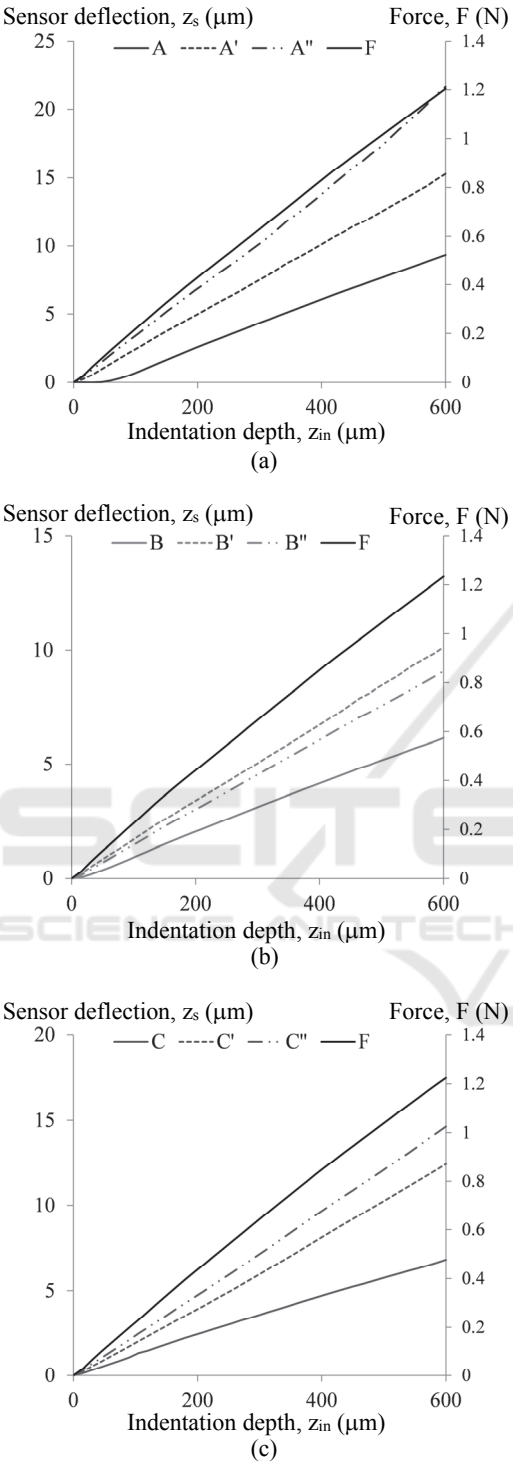

Figure 3: Sensor deflections, $z_{s\text{-}i}$, as a function of indentation depth, z_{in}, with a 11mm-long and 0.8mm-in-diameter cylinder probe above the transducer column (a) A, A′ and A″ (b) B, B′ and B″, (c) C, C′ and C″, respectively.

freezer. The frozen tumor tissues defrosted at room temperature for 2 hours to recover tissue flexibility before the experiment was performed. As shown in Figure 4, the two prepared mice tumor tissues are labelled as tumor tissue #1and tumor tissue #2, respectively. Coincident with the sensing region of the sensor, the tissue region highlighted in each tumor tissue is the palpated region.

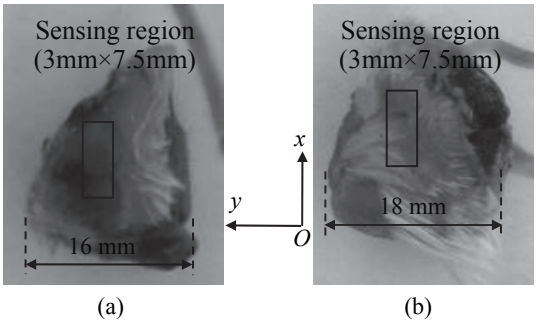

Figure 4: Pictures of the prepared mice tumor tissues (a) tumor tissue #1 and (b) tumor tissue #2.

3.2 Palpation Rationale

The experimental setup for palpating a tumor tissue using the tactile sensor is shown in Figure 5. With the sensor mounted on its end effector, a Mitsubishi RV 3S robot is used to control the motion of the sensor during palpation. With a displacement repeatability of ±20μm, the robot offers the capability of position control and 6 DOFs of the sensor. The rest of the setup is the same as the setup for characterizing the sensor. Additionally, the six-axis force/torque sensor is incorporated into the setup for monitoring the accompanying reaction force of a tumor tissue, in response to an indentation depth input.

As shown in Figure 6, after being aligned on a tissue region of a tumor tissue, the tactile sensor is pressed against the tissue with an indentation depth, z_{in}, and the distributed deflection, $z_{s\text{-}i}$, of the sensor is acquired concurrently. Based on the characterized relation between the deflection on top of a sensing-plated and the deflection at its bottom, the top deflection, $z_{top\text{-}i}$, is obtained. Since the sensing-plates are designed to have the same stiffness, the variation in bottom deflection among the sensing plates originates from the stiffness distribution of a tissue region. Since a tumor is stiffer than its surrounding healthy tissue, a large deflection at a sensing-plate indicates the location of the tumor in a tissue. Additionally, the overall reaction force acting on the tissue can be used to avoid possible damage to the tissue during palpation.

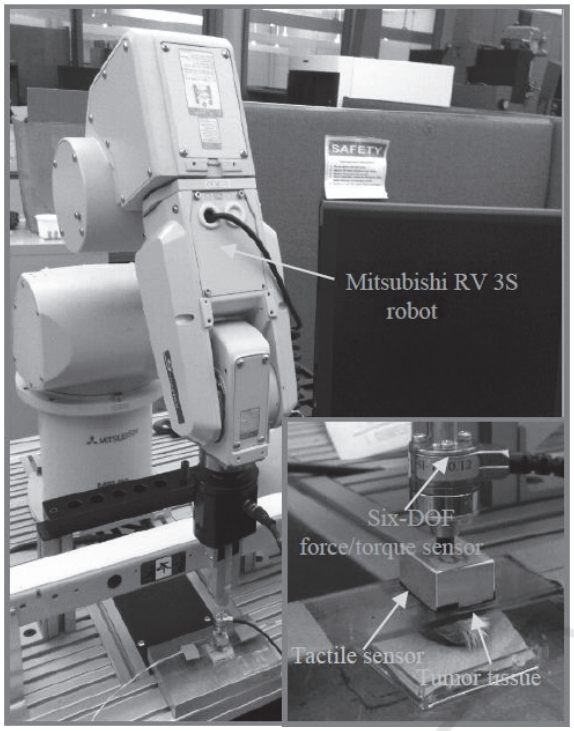

Figure 5: Picture of experimental setup for robotic-assisted tumor localization.

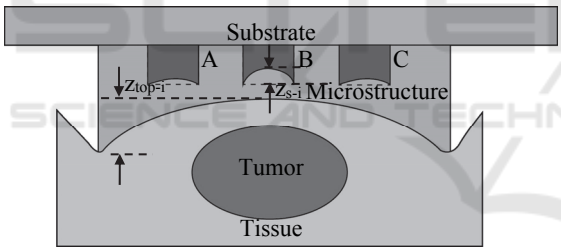

Figure 6: Schematic of palpation on a tumor tissue via a 2D microfluidic-based tactile sensor (drawn not to scale for clear illustration).

3.3 Tissue Palpation Protocol

Prior to palpation, the sensor is visually aligned on the surface of a tissue region with the best achievable normal contact, via the robotic arm. The resistances of the sensor after being aligned are measured and are treated as the initial resistances. Later on, the resistance change is calculated relative to the initial resistance for each palpation to compensate for the performance variations among the transducers resulting from fabrication variation and the misalignment. Afterward, the sensor palpates a tissue region with a pre-defined indentation pattern. The position of the sensor after being aligned is treated as its initial position. As shown in Figure 7, each time the sensor is brought down to an indentation depth of 0.2mm at a speed of 0.25mm/s and is held at the position for 5s, until reaching the final indentation depth of 4mm.

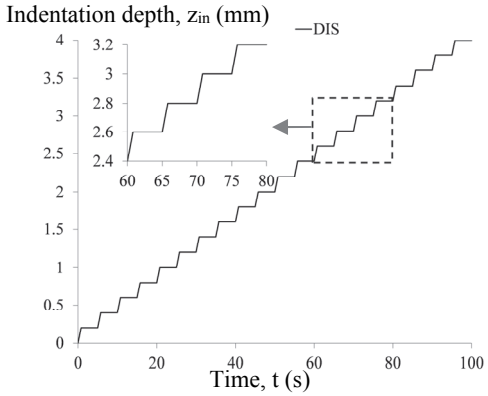

Figure 7: Pre-defined indentation pattern, z_{in}, for palpating a tumor tissue via the tactile sensor.

4 MEASURED RESULTS

4.1 Noise Removal

The raw transducer outputs are visibly corrupted with significant noise. A spectral analysis is performed on these signals, which reveals broadband noise that is uncorrelated across the transducers. Additionally a significant amount of main noise (60Hz) and its harmonics is also present. To remove the presence of broadband interference from the transducer DC voltage outputs, in addition to removing the mains noise and its harmonics, a 4th order Chebyschev Type II low pass filter is created in MATLAB. The Type II filter is chosen as this minimizes ripples in the passband. A passband corner frequency of 10Hz is selected because the robotic arm is not expected to apply a changing pressure at a rate greater than ten times per second. A 40dB decrease in the stopband power was specified. In order to minimize the edge effects inherent in any digital filtering, the first sample is used to initially populate the entire filter structure.

For illustrating the effectiveness of the low pass filter, comparisons of the raw signal of DC voltage output of transducer A, denoted as “A”, with the signal after filtering, denoted as “A_filter”, from the measured results on tumor tissue #1 are presented in Figure 8. The signal appears significantly cleaner after employing the low pass filter. The originally recorded transducer voltage outputs on the two

tumor tissues are all processed by the same noise removal algorithm.

4.2 Measured Deflection/ Depth Slope Distribution for Tumor Localization

In Figure 9, the measured distributed deflection of the sensor on the two tumor tissues as a function of time, together with the indentation depth, are described. Since the LabVIEW program for collecting the data from the sensor starts prior to the program for controlling the robot, the end time of the data acquisition is longer than 100 seconds. As can be seen in Figure 9(a), the transducers, A and B, display larger deflection than the rest transducers, while the transducers, A′ and A″ exhibit larger deflection than the rest transducers in Figure 9(b). Figure 9(c) and 9(d) illustrate the sensor deflection of selected transducers in a short time span. Evidently, the relaxation behaviour (viscosity) during the hold time varies between the two tumor tissues, with tumor tissue #1 being less viscous.

Although the same sensor and the same setup are used to palpate the two tumor tissues, the results on tumor tissue #2 are dramatically noisier than the

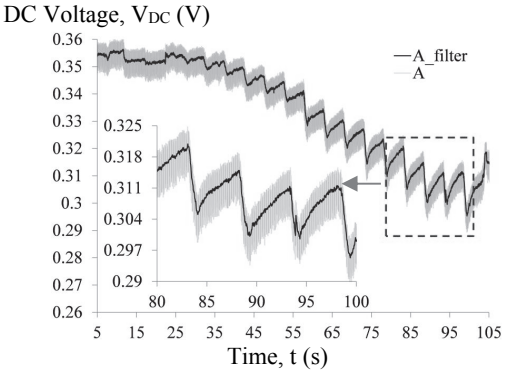

Figure 8: Comparison of the DC voltage, V_{DC}, output of transducer A of the 2D tactile sensor as a function of time.

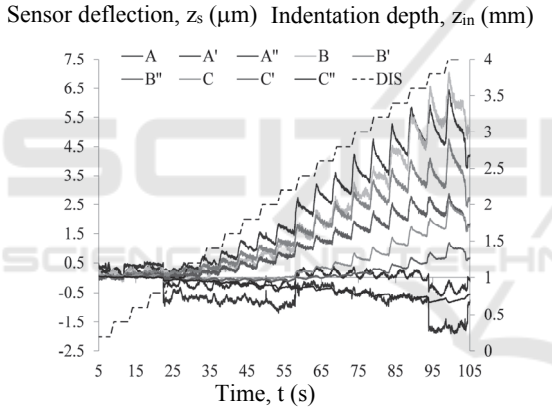

(a)

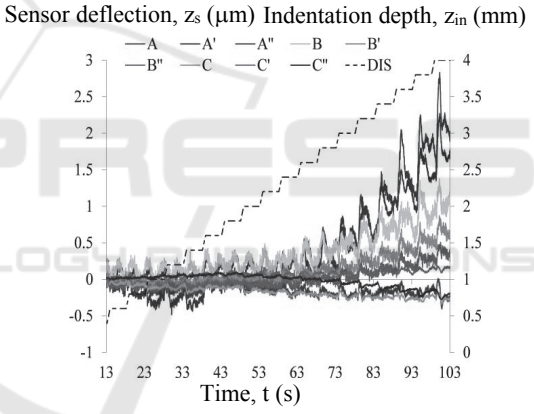

(b)

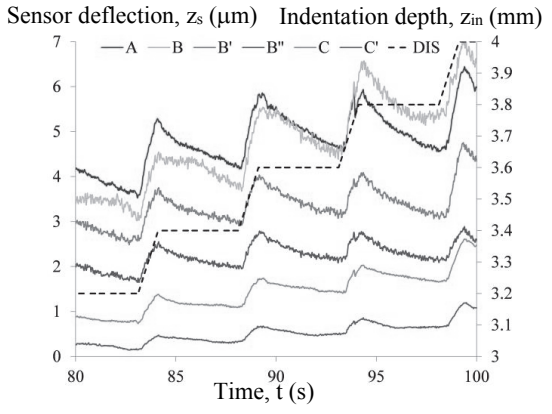

(c)

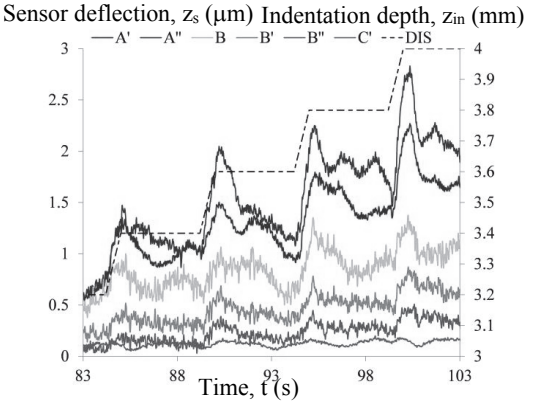

(d)

Figure 9: Distributed defelction, z_s, of the tactile sensor as a function of time, t, on the measured results of (a), (c)tumor #1 and (b), (d)tumor #2, respectively.

results on tumor tissue #1, simply because the tumor tissue #2 is soft and thus the sensor works in its lower end of deflection range, as will be seen later on.

To alleviate the error associated with uncertainty in contact point, the slope of sensor deflection, z_s, and indentation depth, z_{in}, is used to represent the stiffness distribution of a tissue region and consequently localize a tumor. The measured sensor deflection and the overall palpation force as a function of indentation depth are shown in Figures 10(a) and 10(b). Under the same indentation depth, the palpation force of tumor tissue #2 is much smaller than that of tumor tissue #2, indicating that tumor tissue #2 is softer than tumor tissue #1. The palpation results need to be illustrated in a convenient and straightforward manner. Toward this end, the slope, z_s/z_{in} (μm/mm), of sensor deflection, z_s, and indentation depth, z_{in}, the slope error and the percentage error in the slope, $\delta(z_s/z_{in})/(z_s/z_{in})$, with the one in bold font indicating the highest slope, are summarized in Table 1. To minimize the measurement errors at the lower end of the sensor's deflection range, the indentation depth ranges of 1.5mm~4mm and 2.5mm~4mm are used to extract the slopes for the tumor tissues #1 and #2, respectively. Based on the slope values of the transducer array in Table 1, color maps are generated on the tumor tissues, as shown in Figure 11. These color maps utilize the visual color to indicate the levels of localized slope experienced by the sensor, with red indicating the highest slope and blue indicating the lowest slope. As can be seen in Figure 11(a), the transducer B displays a much larger slope than the rest transducers, indicating that the tumor embedded in tissue #1 is located at the site of this transducer. In contrast, the transducer A″ exhibits a much larger slope than the rest transducers in Figure 11(b), implying that the tumor is at the site of this transducer. Since the two tumor tissues have similar surface profiles with similar small curvatures,

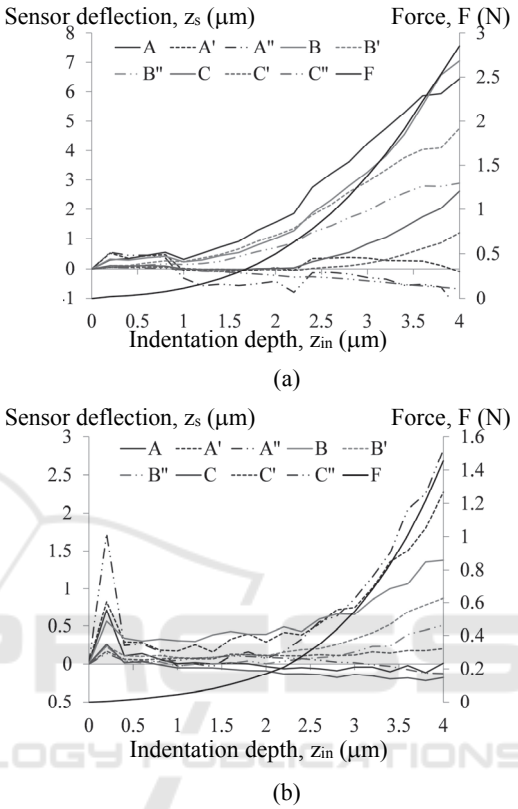

Figure 10: Distributed deflection, z_s, and the overall palpation force, F, of the tactile sensor as a function of the indentation depth, z_{in}, on the measurements of (a) tumor #1 and (b) tumor #2, respectively.

Table 1: Measured deflection/depth slope (z_{s-i}/z_{in}), slope error ($\delta(z_{s-i}/z_{in})$) and percentage error in the slope ($\delta(z_{s-i}/z_{in})/(z_{s-i}/z_{in})$) of two tumor tissues via a 2D microfluidic-based tactile sensor.

	Tumor #1			Tumor #2		
	z_{s-i}/z_{in}	$\delta(z_{s-i}/z)$	$\delta(z_{s-i}/z)/(z_{s-i}/z)$	z_{s-i}/z_{in}	$\delta(z_{s-i}/z)$	$\delta(z_{s-i}/z)/(z_{s-i}/z)$
A	2.375	0.092	3.9%	0.030	0.046	153.8%
A′	-0.232	0.057	24.7%	1.295	0.113	8.7%
A″	-0.626	0.140	22.3%	**1.833**	**0.111**	**6.0%**
B	**3.355**	**0.194**	**5.8%**	0.673	0.063	9.4%
B′	1.777	0.075	4.2%	0.541	0.027	5.0%
B″	1.123	0.081	7.2%	0.352	0.030	8.5%
C	1.446	0.098	6.7%	-0.035	0.023	63.8%
C′	0.709	0.080	11.3%	0.072	0.012	16.1%
C″	-0.263	0.007	2.5%	-0.142	0.013	9.1%

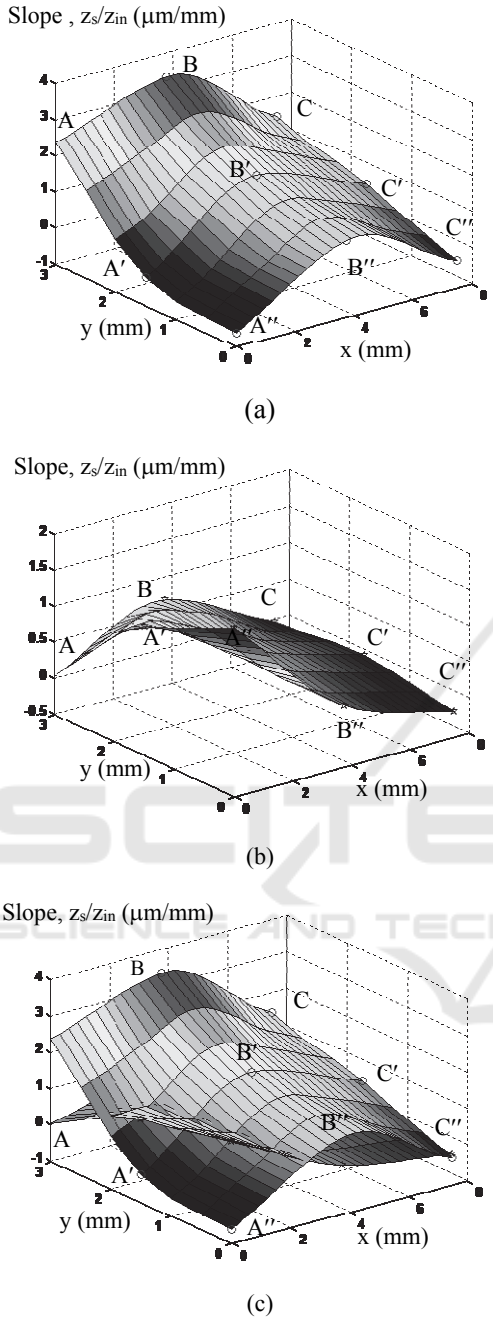

Figure 11: Color maps based on the slopes, (z_s/z_{in}, μm/mm) of sensor deflection, z_s, versus indentation depth, z_{in}, on the two tumor tissues (a) tumor tissue #1, (b) tumor tissue #2 and (c) comparison of the two tumor tissues.

it can be concluded that the slope distribution represents the stiffness distribution of a tumor tissue, instead of its surface profile. In Figure 10(a), transducer A has a larger deflection than transducer B, but the deflection of transducer A does not increase with the indentation depth as fast as the deflection of transducer B. This indicates that transducer A is located at a tissue site higher than the rest tissue sites, but this tissue site has a lower stiffness than that of transducer B. As such, using the slope distribution is more accurate for tumor localization. The comparison between the two tissues in Figure 11(c) evidently illustrates that tumor tissue #1 is stiffer than tumor tissue #2, which is consistent with the conclusion drawn from the overall palpation force difference in Figure 10.

Here, some practical concerns about using this 2D tactile sensor for tissue palpation are discussed. First, as compared with those tactile sensor arrays or individual sensors for tissue palpation, this 2D sensor is much more immune to misalignment errors, simply because one whole PDMS microstructure with embedded transducer array palpates a tissue region in a continuous manner and thus similar small tilt angles are formed across the transducer array. Second, the surface profile may introduce some variation in the slopes across a tissue region. Both tumor tissues contain a slightly convex surface profile, which is not expected to yield a high slope at the center of the tissue region. However, a convex surface profile with a small radius of curvature may give rise to false identification of a tumor at the center. As such, in the future, the effect of the surface profile of a tissue region needs to be removed from the measured slopes. Third, to minimize the percentage error in the slope, the sensor design needs to be tailored so that the stiffness of the sensor matches the stiffness of the tissue region. Then, the difference in the slope across a tissue region can more accurately capture the genuine stiffness distribution of the region. Lastly, since we know beforehand that each of the two tissues contains a tumor, we attribute the measured highest slope in a tissue region to the existence of a tumor. In practice, where a tissue region under palpation contains a tumor is not known beforehand, both the surface profile and experimental errors may cause a higher slope at a site on a tissue region than the rest sites. As such, a threshold value on the slope difference in a tissue region needs to be established for accurate tumor identification. This threshold value needs to factor in the elasticity of a tissue itself and the tumor variables (i.e., elasticity, size and depth).

5 CONCLUSIONS

In this paper, a 2D microfluidic-based tactile sensor is mounted on a robot and utilized to palpate two

mice tumor tissues. The sensor entails a 3×3 sensing-plate/transducer array built into a single PDMS microstructure. The distributed deflection acting on the top of the sensing-plate array translates to resistance changes of the transducer array underneath. The continuity of the sensing-plate array configuration overcomes the varying tilt angles across a tissue region encountered by an individual sensor or a sensor array, thus avoiding distorting the genuine stiffness distribution of the tissue region. In palpating a mice tissue, the input is the indentation depth controlled by the robot and the output is the sensor deflection at the locations of the transducer array.

Although the robot introduces a significant amount of noise to the recorded dada, a noise filter is able to effectively remove the noise, indicating that the sensor is feasible to be integrated into a robotic-assisted system. The palpation results are interpreted in terms of the slope distribution of the sensor deflection versus indentation depth, with the highest slope indicating the location of a tumor. Although the two mice tissues have similar surface profiles, the slope distribution varies dramatically between them and thus is believed to arise from the existence of tumors in them, validating the feasibility of using this sensor for palpating true tumor tissues. Future work will focus on improving the sensor design with a suitable working deflection range to reduce slope errors and reducing the sensor size for fitting in RMIS. In addition, more tissue samples will be measured using the presented detection method to verify its repeatability.

ACKNOWLEDGEMENTS

The authors would like to acknowledge the financial support for this work from the National Science Foundation, CMMI, under Grant No. 1265785.

REFERENCES

Anastassopoulos, G. T., Lytras, J. G., Sunaric, M. M., Moulianitis, V. C., Panteliou, S. D., Bekos, A., Kalinderis, N. and Hatzichristou, D., 2001. Optical device for prostate cancer detection. In *6th National Congress of Mechanics* (p.381).

Beccani, M., Di Natali, C., Benjamin, C. E., Bell, C. S., Hall, N. E. and Valdastri, P., 2015. Wireless tissue palpation: Head characterization to improve tumor detection in soft tissue. *Sensors and Actuators A: Physical*, 223, pp.180-190.

Dargahi, J. and Najarian, S., 2003. An integrated force-position tactile sensor for improving diagnostic and therapeutic endoscopic surgery. *Bio-medical materials and engineering*, 14(2), pp.151-166.

Girão, P. S., Ramos, P. M. P., Postolache, O. and Pereira, J. M. D., 2013. Tactile sensors for robotic applications. *Measurement*, 46(3), pp.1257-1271.

Gu, W., Cheng, P., Ghosh, A., Liao, Y., Liao, B., Beskok, A. and Hao, Z., 2013a. Detection of distributed static and dynamic loads with electrolyte-enabled distributed transducers in a polymer-based microfluidic device. *Journal of Micromechanics and Microengineering*, 23(3), p.035015.

Gu, W., Cheng, P., Palmer, X. L. and Hao, Z., 2013b. Concurrent spatial mapping of the elasticity of heterogeneous soft materials via a polymer-based microfluidic device. *Journal of Micromechanics and Microengineering*, 23(10), p.105007.

Guthart, G. and Salisbury Jr, J.K., 2000. The intuitive™ telesurgery system: Overview and application. In *International Conference on Robotics and Automation* (pp. 618-621).

Konstantinova, J., Jiang, A., Althoefer, K., Dasgupta, P. and Nanayakkara, T., 2014. Implementation of tactile sensing for palpation in robot-assisted minimally invasive surgery: A review. *Sensors Journal, IEEE*, 14(8), pp.2490-2501.

Krouskop, T. A., Wheeler, T. M., Kallel, F., Garra, B. S. and Hall, T., 1998. Elastic moduli of breast and prostate tissues under compression. *Ultrasonic imaging*, 20(4), pp.260-274.

Lanfranco, A. R., Castellanos, A. E., Desai, J. P. and Meyers, W. C., 2004. Robotic surgery: a current perspective. *Annals of surgery*, 239(1), p.14.

Ottermo, M. V., Øvstedal, M., Langø, T., Stavdahl, Ø., Yavuz, Y., Johansen, T. A. and Mårvik, R., 2006. The role of tactile feedback in laparoscopic surgery. *Surgical Laparoscopy Endoscopy & Percutaneous Techniques*, 16(6), pp.390-400.

Panteliou, S. D., Sunaric, M. M., Sarris, J., Anastassopoulos, G., Lytras, J. and Hatzichristou, D. G., 2000. Design of a device for the objective assessment of the mechanical properties of the prostate gland. In *International Conference on Role of Mesomechanics for the Development of Science and Technology*.

Puangmali, P., Althoefer, K., Seneviratne, L. D., Murphy, D. and Dasgupta, P., 2008. State-of-the-art in force and tactile sensing for minimally invasive surgery. *Sensors Journal, IEEE*, 8(4), pp.371-381.

Schostek, S., Schurr, M. O. and Buess, G. F., 2009. Review on aspects of artificial tactile feedback in laparoscopic surgery. *Medical Engineering & Physics*, 31(8), pp.887-898.

Su, Z., Fishel, J. A., Yamamoto, T. and Loeb, G. E., 2012. Use of tactile feedback to control exploratory movements to characterize object compliance. *Frontiers in neurorobotics*, 6.

Talasaz, A. and Patel, R. V., 2013. Integration of force reflection with tactile sensing for minimally invasive

robotics-assisted tumor localization. *Haptics, IEEE Transactions on*, 6(2), pp.217-228.

Tiwana, M. I., Redmond, S. J. and Lovell, N. H., 2012. A review of tactile sensing technologies with applications in biomedical engineering. *Sensors and Actuators A: physical*, 179, pp.17-31.

Trejos, A. L., Jayender, J., Perri, M. P., Naish, M. D., Patel, R. V. and Malthaner, R. A., 2009. Robot-assisted tactile sensing for minimally invasive tumor localization. *The International Journal of Robotics Research*.

Uranues, S., Maechler, H., Bergmann, P., Huber, S., Hoebarth, G., Pfeifer, J., Rigler, B., Tscheliessnigg, K. H. and Mischinger, H. J., 2002. Early experience with telemanipulative abdominal and cardiac surgery with the Zeus™ Robotic System. *European Surgery*, 34(3), pp.190-193.

Wanninayake, I. B., Dasgupta, P., Seneviratne, L. D. and Althoefer, K., 2013. Air-float palpation probe for tissue abnormality identification during minimally invasive surgery. *Biomedical Engineering, IEEE Transactions on*, 60(10), pp.2735-2744.

Yang, Y., Shen, J. and Hao, Z., 2015a. A two-dimensional microfluidic-based tactile sensor for tissue palpation application under the influence of misalignment. In *ASME 2015 International Technical Conference and Exhibition on Packaging and Integration of Electronic and Photonic Microsystems collocated with the ASME 2015 13th International Conference on Nanochannels, Microchannels, and Minichannels*(pp.V003T05A001-V003T05A001). American Society of Mechanical Engineers.

Yang, Y., Shen, J. and Hao, Z., 2015b. A two-dimensional (2D) distributed-deflection sensor for tissue palpation with correction mechanism for its performance variation. *under review*.

Zhao, S., Parks, D. and Liu, C., 2013. Design and Modeling of a Wide Dynamic-Range Hardness Sensor for Biological Tissue Assessment. *Sensors Journal, IEEE*, 13(12), pp.4613-4620.